



Deposited via The University of Leeds.

White Rose Research Online URL for this paper:

<https://eprints.whiterose.ac.uk/id/eprint/151947/>

Version: Accepted Version

Article:

Bridgestock, L, Hsieh, Y-T, Porcelli, D et al. (2018) Controls on the barium isotope compositions of marine sediments. *Earth and Planetary Science Letters*, 481. pp. 101-110. ISSN: 0012-821X

<https://doi.org/10.1016/j.epsl.2017.10.019>

© 2017, Elsevier. This manuscript version is made available under the CC-BY-NC-ND 4.0 license <http://creativecommons.org/licenses/by-nc-nd/4.0/>.

Reuse

This article is distributed under the terms of the Creative Commons Attribution-NonCommercial-NoDerivs (CC BY-NC-ND) licence. This licence only allows you to download this work and share it with others as long as you credit the authors, but you can't change the article in any way or use it commercially. More information and the full terms of the licence here: <https://creativecommons.org/licenses/>

Takedown

If you consider content in White Rose Research Online to be in breach of UK law, please notify us by emailing eprints@whiterose.ac.uk including the URL of the record and the reason for the withdrawal request.

1 **Controls on the barium isotope compositions of marine sediments**

2

3 Luke Bridgestock^{a*}, Yu-Te Hsieh^a, Donald Porcelli^a, William B. Homoky^a, Allison

4 Bryan^a, Gideon M. Henderson^a

5

6 ^aDepartment of Earth Sciences, University of Oxford, South Parks Road, Oxford,

7 OX1 3AN, UK

8

9 *Corresponding author; luke.bridgestock@earth.ox.ac.uk

10

11 **Keywords:** Barium isotopes; marine sediments; marine barium cycle; paleo-

12 oceanography; GEOTRACES

13

14 **Highlights:**

15 1. Detrital and authigenic Ba in marine sediments have distinct isotope

16 compositions

17 2. Sinking particles predicted to have similar isotope compositions to authigenic

18 Ba

19 3. Ba removal to sediments has an isotope fractionation of $\Delta^{138/134}\text{Ba} \approx +0.4$ to

20 +0.5

21 4. Sedimentary Ba isotope compositions record perturbations to upper ocean Ba

22 cycling

23

24 Abstract; 254 words

25 Main text; 5,885 words

26 **Abstract**

27 The accumulation of barium (Ba) in marine sediments is considered to be a robust
28 proxy for export production, although this application can be limited by uncertainty in
29 BaSO₄ preservation and sediment mass accumulation rates. The Ba isotope
30 compositions of marine sediments could potentially record insights into past changes
31 in the marine Ba cycle, which should be insensitive to these limitations, enabling
32 more robust interpretation of sedimentary Ba as a proxy. To investigate the controls
33 on the Ba isotope compositions of marine sediments and their potential for paleo-
34 oceanographic applications, we present the first Ba isotope compositions results for
35 sediments, as well as overlying seawater depth profiles collected in the South
36 Atlantic. Variations in Ba isotope compositions of the sediments predominantly
37 reflect changes in the relative contributions of detrital and authigenic Ba sources, with
38 open-ocean sediments constraining the isotope composition of authigenic Ba to be
39 $\delta^{138/134}\text{Ba} \approx +0.1 \text{ ‰}$. This value is consistent with the average isotope composition
40 inferred for sinking particulate Ba using simple mass balance models of Ba in the
41 overlying water column and is hypothesized to reflect the removal of Ba from the
42 upper water column with an associated isotopic fractionation of $\Delta^{138/134}\text{Ba}_{\text{diss-part}} \approx$
43 $+0.4$ to $+0.5$. Perturbations to upper ocean Ba cycling, due to changes in export
44 production and the supply of Ba via upwelling, should therefore be recorded by the
45 isotope compositions of sedimentary authigenic Ba. Such insights will help to
46 improve the reliable application of Ba accumulation rates in marine sediments as a
47 proxy for past changes in export production.

48

49

50

51 **1. Introduction**

52

53 Interest in the marine biogeochemical cycle of barium (Ba) has been largely
54 motivated by its potential to trace aspects of the marine organic carbon cycle. In
55 particular, the accumulation of Ba in marine sediments is considered to be a robust
56 proxy for export production in the modern (e.g. Eagle et al., 2003) and past oceans
57 (e.g. Paytan & Griffiths, 2007). Inventories of suspended particulate Ba have also
58 been used to study the remineralization of exported organic carbon in mesopelagic
59 waters (e.g. Cardinal et al., 2005, Jacquet et al., 2015). The precipitation of barite
60 (BaSO_4) is the dominant oceanic sink of Ba, and forms the basis of these proxy
61 applications (Dehairs et al., 1980). The vast majority of the global ocean is under-
62 saturated with respect to this mineral, therefore BaSO_4 precipitation is thought to
63 occur in supersaturated micro-environments during the bacterial decay of organic
64 aggregates, and/or through the dissolution of acantharian celestite (SrSO_4) skeletons
65 (Monnin et al., 1999, Bishop, 1988, Ganeshram et al., 2003, Bernstein & Byrne,
66 2004). The precipitation of BaSO_4 is considered to predominantly occur within
67 mesopelagic waters, where the majority of organic carbon remineralization takes
68 place, although it can potentially occur at any depth throughout the water column
69 (Dehairs et al., 1980, Dymond et al., 1992, Legeleux & Reyss, 1996, Cardinal et al.,
70 2005, van Beek et al., 2007, 2009).

71 The use of sedimentary Ba accumulation rates as a proxy for export
72 production is founded on the observation that fluxes of particulate Ba sinking through
73 the water column are typically correlated with those of particulate organic carbon,
74 although there is significant variability in the ratio of these two components both
75 spatially and temporally (Dymond et al., 1992, Francois et al., 1995, Dymond &

76 Collier, 1996, Dehairs et al., 2000, McManus et al., 2002, Balakrishnan Nair et al.,
77 2005, Sternberg et al., 2007). Once buried below the sediment-water interface, BaSO₄
78 particles appear to be well preserved (Paytan & Kastner, 1996), provided that pore
79 waters are not depleted in SO₄²⁻ (e.g. Torres et al., 1996). High preservation rates of
80 BaSO₄, at least in oxic sediments, compared to biogenic sedimentary components
81 such as organic carbon, CaCO₃ and opal, make Ba accumulation rates a robust proxy
82 for export production (e.g. Dymond et al., 1992).

83 Preservation rates of BaSO₄ at the sediment-water interface however are
84 known to be variable in the modern ocean (Fagel et al., 2002). This is a source of
85 uncertainty for reconstructions of export production in the past, which could be
86 exacerbated by changes in the saturation state of the ocean with respect to BaSO₄
87 through time (e.g. Dickens et al., 2003). The concentration of Ba in marine sediments
88 is also significantly affected by dilution due to the accumulation of other sedimentary
89 components (e.g. CaCO₃), requiring conversion to Ba accumulation rates using age
90 models or constant flux proxies such as ²³⁰Th or extraterrestrial ³He (Paytan &
91 Griffith, 2007). Uncertainty in establishing bulk sediment accumulation rates can
92 produce significant uncertainty in Ba accumulation rates, which can affect the
93 apparent timing and magnitude of inferred changes in export production (Anderson &
94 Winckler, 2005, Torfstein et al., 2010). Detrital inputs of aluminosilicate minerals can
95 also compromise export production estimates derived from Ba accumulation rates,
96 particularly in settings close to the continental margin (Dymond et al., 1992, Reitz et
97 al., 2004),

98 Improved understanding of the ocean and sedimentary cycling of Ba would be
99 beneficial for reliable application of the Ba proxy for export production. Recent
100 studies have shown that the removal of Ba from the upper ocean is associated with an

101 isotopic fractionation with a preference for the lighter isotopes (Horner et al., 2015,
102 Bates et al., 2017, Hsieh & Henderson, 2017). Barium isotope composition variations
103 therefore have the potential to offer insights into the different sources and sinks of Ba
104 in the water column. The Ba isotope compositions of marine sediments may record
105 insights into changes in the marine Ba cycle in the past, which should be insensitive to
106 variable BaSO₄ preservation and dilution by biogenic sedimentary components,
107 enabling more robust interpretations of the Ba proxy for export production. However,
108 the magnitude of the isotope fractionation accompanying Ba removal from the ocean
109 is currently poorly constrained, as are the controls on the Ba isotope compositions of
110 marine sediments. To address these issues and to investigate the potential of Ba
111 isotope compositions of marine sediments for paleo-oceanographic reconstructions,
112 we present the first Ba isotope composition data for marine sediments, in addition to
113 overlying seawater depth profiles from the South Atlantic.

114

115 **2. Samples and hydrography**

116

117 Seawater and sediment samples analyzed in this study were collected during
118 the JC068 expedition (December, 2011 – January, 2012) as part of the GEOTRACES
119 GA10 section, on board the RSS James Cook (Fig. 1).

120 A total of 49 seawater samples were measured for Ba concentrations and
121 isotope compositions in this study, taken from four water-column profiles, extending
122 from the continental slope of the Uruguayan margin (stations 21 and 22), to the
123 Argentine Basin (station 18) and mid Atlantic Ridge (station 12). In addition Ba
124 concentration and isotope composition results for a seawater depth profile collected at
125 station 20 previously published by Hsieh & Henderson (2017) are included. Six

126 sediment cores were collected from the continental shelf and slope of the Uruguayan
127 margin, the abyssal plain of the Argentine Basin and the mid Atlantic Ridge (Fig. 1).
128 A total of 93 sediment samples from these cores were measured for Ba and Al
129 concentrations, with 58 of these samples analyzed for Ba isotope compositions.

130 The water masses encountered on the GEOTRACES GA10 section are
131 distinguished by their distinct salinity values (Fig. 1b). Hydrographic data for this
132 cruise transect are available as part of the GEOTRACES data product (Mawji et al.,
133 2015).

134 Seawater was collected using either a stainless steel or titanium rosette each
135 equipped with 24 Ocean Test Equipment sampling bottles. Seawater was filtered on-
136 board into acid-cleaned polypropylene bottles using 0.45 μm Acropak capsule filters,
137 before being acidified to $\text{pH} \approx 1$ to 2 by addition of distilled HCl. Sediment cores
138 were collected using a Bowers and Connelly Megacore, retrieving between 10 and 36
139 cm of the surface sediments with intact sediment-water interfaces (Homoky et al.,
140 2013). Following extraction of the pore waters, the residual sediment was divided at 1
141 to 2 cm depth intervals using a Teflon sheet. Sediments from the individual depth
142 intervals were subsequently freeze-dried and homogenized by agate pestle and mortar.
143 Pore water data for NO_3^- and Fe indicate that pore waters over the sampled depth
144 ranges of the sediment cores are not likely to be depleted in SO_4^{2-} (Supplementary
145 Material).

146

147 **3. Analytical techniques**

148

149 Sample preparation and analyses were conducted at the University of Oxford.

150 The Ba isotope compositions of seawater and sediment samples were determined

151 using thermal ionization mass spectrometry (TIMS), with the application of a ^{137}Ba –
152 ^{135}Ba double spike to correct for instrumental mass bias (Hsieh & Henderson, 2017).
153 Approximately 50 ml of seawater was accurately weighed and equilibrated with a
154 known quantity of Ba double spike solution. The Ba was then co-precipitated with
155 CaCO_3 by addition of 3 ml of a 0.9 M Na_2CO_3 solution, prior to purification by cation
156 exchange chromatography (Supplementary Material; Foster et al., 2004, Nan et al.,
157 2015, Horner et al., 2015). Organics leached from the cation exchange resin were
158 oxidized by the sequential addition and evaporation of 7.5M HNO_3 and 9.8M H_2O_2 .
159 The procedural blank was typically < 1 ng ($n = 5$); however on two occasions it was
160 slightly higher at 3 and 4 ng of Ba. These values, typically representing < 0.4 %, and
161 in the worst case < 1.6 % of the Ba processed in the samples (≈ 250 to 700 ng), are
162 considered to have a negligible impact on the quality of the data, and hence no blank
163 corrections were applied.

164 For the sediment samples, between 0.3 to 0.9 g of powdered sediment was
165 accurately weighed into Teflon vials, prior to total digestion in 1.25 ml 16M HNO_3 +
166 3.75 ml 12M HCl at 60°C , followed by 3 ml 28M HF + 2.25 ml 11.6M HClO_4 at
167 150°C and finally 2 ml 11.6M HClO_4 at 150°C to 180°C , after Homoky et al. (2011).
168 Residual HClO_4 was removed by the repeated addition and evaporation of 1 – 2 ml
169 16M HNO_3 at 150°C to 200°C . The digested samples were then re-dissolved in 10 ml
170 0.5M HNO_3 . The Ba and Al contents of the digested solutions were determined using
171 magnetic sector inductively coupled plasma mass spectrometry (ICP-MS; Thermo
172 Scientific, Element 2), with the addition of Rh as an internal standard.

173 Aliquots of the digested solutions, containing about 1000 ng Ba, were taken
174 for determination of Ba isotope compositions. Appropriate quantities of the ^{137}Ba –
175 ^{135}Ba double spike solution were equilibrated with the sample aliquots prior to

176 purification of Ba by cation exchange chromatography (Supplementary Material;
177 Foster et al., 2004, Hsieh & Henderson, 2017). Organics leached from the cation
178 exchange resin were subsequently oxidized by the sequential addition and evaporation
179 of 7.5M HNO₃ and 9.8M H₂O₂. The procedural blank was consistently determined to
180 be < 1.6 ng (n = 9), representing < 0.16 %, of the Ba processed in the samples, hence
181 no blank corrections were applied.

182 The purified Ba was loaded onto previously outgassed single Re filaments,
183 along with 1 µl of a Ta₂O₅ – H₃PO₄ activator gel as described by Hsieh & Henderson
184 (2017). More stable ion beams were achieved by loading the activator gel onto the
185 filament before the sample. The Ba isotope measurements were conducted using a
186 Thermo Scientific TRITON TIMS instrument. Filaments were heated to between
187 1500°C and 1550°C within about 30 to 40 mins. Higher and more stable ion beams
188 were typically achieved if filaments were initially heated to approximately 1600°C,
189 before cooling to between 1500°C and 1550°C. The resulting ion beam intensities
190 were typically 5 to 8 V for the most abundant isotope, ¹³⁸Ba. During each analysis, ion
191 beams at atomic masses 134 (Ba), 135 (Ba), 136 (Ba), 137 (Ba), 138 (Ba), 139 (La)
192 and 140 (Ce) were monitored simultaneously using Faraday cups equipped with 10¹¹
193 Ω resistors. Following a peak center, ion beams were collected in 54 blocks of 10
194 integrations lasting 8.4 seconds each. Between each block, ion beams were deflected
195 to measure the electronic baseline. The ion beams at atomic masses 139 (La) and 140
196 (Ce) were monitored to assess potential isobaric inferences on ¹³⁶Ba and ¹³⁸Ba, and
197 during all analyses displayed no detectable signal.

198 The raw isotopic ratios were processed offline to correct for instrumental mass
199 bias (Hsieh & Henderson, 2017). The Ba isotope compositions are expressed as

200 $\delta^{138/134}\text{Ba}$ values, which are parts per thousand deviations from a Ba standard
201 reference material (SRM) NIST 3104a (eqn. 1).

202

$$203 \quad \delta^{138/134}\text{Ba} = \left(\frac{{}^{138}\text{Ba}/{}^{134}\text{Ba}_{\text{sample}}}{{}^{138}\text{Ba}/{}^{134}\text{Ba}_{\text{NIST3104a}}} - 1 \right) \times 1000 \quad (1)$$

204

205 The isotopic results were also used to obtain Ba concentrations of seawater samples
206 by isotope dilution.

207

208 **4. Results**

209

210 Repeat analyses of SRM NIST3104a, at similar ion beam intensities to those
211 of sample measurements result in external reproducibility of $\delta^{138/134}\text{Ba}$ of ± 0.03 , or
212 better (2SD; see Supplementary Material). This level of uncertainty is taken to
213 represent that of the samples, and is justified by the agreement displayed by duplicate
214 measurements of certain seawater (Fig. 2; Fig. 3; Supplementary Data 1) and
215 sediment samples (Fig. 4; Supplementary Data 2). Further validation is provided by 7
216 repeat analyses of two different seawater samples collected in the North Atlantic,
217 which yield external reproducibility for $\delta^{138/134}\text{Ba}$ of ± 0.003 and ± 0.01 (2SD; Hsieh
218 & Henderson, 2017). The Ba concentrations of these replicate seawater analyses
219 display a reproducibility of ± 2 to 3% (RSD) which is taken to represent the
220 uncertainty of the seawater Ba concentrations.

221

222 *4.1 Dissolved Ba concentrations and isotope compositions of seawater samples*

223

224 From the surface to the deep ocean, dissolved Ba concentrations increase from
225 approximately 40 to 100 nmol kg⁻¹, while $\delta^{138/134}\text{Ba}$ values decrease from
226 approximately +0.6 to +0.2 ‰ (Fig. 2; Supplementary Data 1). Consequently, Ba
227 concentrations and $\delta^{138/134}\text{Ba}$ values display a strong negative correlation ($r^2 = 0.89$),
228 with the exception of one anomalous sample from station 20, previously published by
229 Hsieh & Henderson (2017) (Fig. 3).

230 In general, Ba concentrations and $\delta^{138/134}\text{Ba}$ values are relatively constant in
231 the upper 200 to 400 m of the water column (Fig. 2), consistent with previous
232 observations elsewhere in the ocean (Horner et al., 2015, Bates et al., 2017, Hsieh &
233 Henderson, 2017). Laterally along the sampled transect, upper water column (200 m)
234 dissolved Ba concentrations and $\delta^{138/134}\text{Ba}$ values are also uniform at 43.3 ± 4.2 nmol
235 kg⁻¹ and $+0.57 \pm 0.04$ ‰ (2SD; n = 17). Between about 200 to 1000 m water depth,
236 Ba concentrations and $\delta^{138/134}\text{Ba}$ values increase and decrease respectively, to 70 to 80
237 nmol kg⁻¹ and +0.35 to +0.40 ‰ (Fig. 2). Barium concentrations and isotope
238 compositions then remain relatively constant until about 3000 m water depth where
239 Antarctic Bottom Water is encountered, with Ba concentrations increasing to between
240 90 to 110 nmol kg⁻¹, and $\delta^{138/134}\text{Ba}$ values decreasing to about +0.25 ‰. At station 21,
241 a minimum in Ba concentrations (and maximum in $\delta^{138/134}\text{Ba}$ values) is observed at
242 2500 m water depth. Notably a minimum is also observed at this location and depth
243 for the concentrations of the macro-nutrients nitrate, phosphate and silicate, in
244 addition to the micro-nutrient Zn, which presumably represents a hydrographic
245 feature (Wyatt et al., 2014).

246 The general distribution of Ba concentrations and $\delta^{138/134}\text{Ba}$ values, in addition
247 to their co-variance, are consistent with previous results from the North Atlantic,
248 South Atlantic, Southern Ocean and North Pacific (Horner et al. 2015, Bates et al.,

249 2017, Hsieh & Henderson, 2017; Fig. 3). In particular, results for station 12 are in
250 good agreement with the results published by Horner et al. (2015) and Bates et al.
251 (2017) determined at stations 3 and 6 from the GEOTRACES GA10 section
252 (Supplementary Material; Fig.1). Notably, these datasets were produced at a different
253 laboratory, using different analytical techniques (i.e. using multiple collector ICP-MS)
254 than the data presented in this study.

255

256 *4.2 Elemental concentrations and Ba isotope compositions of sediment samples*

257

258 The underlying sediments exhibit lower $\delta^{138/134}\text{Ba}$ values than the seawater
259 samples, ranging between -0.09 to +0.10 ‰ (Fig. 4, Supplementary Data 2). The Ba
260 concentrations of the sediments range from 371 to 1104 $\mu\text{g g}^{-1}$, while Ba/Al mass
261 ratios range between 0.005 and 0.053. In detail, the cores collected on the continental
262 shelf and slope (stations 21, 22, 23 and 24) exhibit relatively low Ba/Al ratios of
263 0.005 to 0.009, while the cores collected on the abyssal plain of the Argentine Basin
264 and the mid Atlantic ridge generally exhibit higher Ba/Al ratios of 0.006 to 0.05 (Fig.
265 4). The $\delta^{138/134}\text{Ba}$ values generally increase with increasing Ba/Al ratio (Fig. 5).

266

267 **5. Discussion**

268

269 *5.1 The isotope compositions of sedimentary Ba sources*

270

271 Inputs of detrital aluminosilicate minerals can provide significant
272 contributions to marine sedimentary Ba inventories, particularly at locations close to
273 the continental margin (e.g. Klump et al., 2000). To assess the importance of detrital

274 Ba inputs to marine sediment, Ba/Al ratios have commonly been applied in previous
275 studies (e.g. Klump et al., 2000, Pfeifer et al., 2001, Reitz et al., 2004). In this study,
276 the lower Ba/Al ratios determined for sediments collected on the continental shelf and
277 slope, compared to those collected on the abyssal plain and mid Atlantic Ridge,
278 reflects higher contributions of detrital Ba to the former sites (Fig. 4). By assuming a
279 Ba/Al ratio for the detrital component of the sediment, it is possible to estimate the
280 fractional contributions of Ba from detrital and non-detrital sources (eqn. 2).

281

$$282 \text{Ba}_{\text{excess}} (\%) = (1 - [(\text{Ba}/\text{Al}_{\text{detrital}} \times \text{Al}_{\text{total}})/\text{Ba}_{\text{total}}]) \times 100 \quad (2)$$

283

284 Where $\text{Ba}_{\text{excess}}$ denotes Ba from non-detrital sources, Ba_{total} and Al_{total} denote the total
285 Ba and Al concentrations of the sediment, and $\text{Ba}/\text{Al}_{\text{detrital}}$ denotes the reference ratio
286 of the detrital material. The accuracy of sedimentary $\text{Ba}_{\text{excess}}$ contribution assessment
287 using this approach primarily depends on the appropriate choice of $\text{Ba}/\text{Al}_{\text{detrital}}$
288 reference ratio, which is known to display regional variations (Klump et al., 2000,
289 Reitz et al., 2004). The lowest Ba/Al ratios for our sediment samples are observed at
290 station 23, with a single sample featuring a Ba/Al ratio of 0.005 and the remainder of
291 about 0.006 (Fig. 4, Fig. 5, Supplementary Data 2). These values provide an upper
292 limit for the appropriate $\text{Ba}/\text{Al}_{\text{detrital}}$ for assessment of $\text{Ba}_{\text{excess}}$ values, and are in good
293 agreement with $\text{Ba}/\text{Al}_{\text{detrital}}$ ratios suggested by Pfeifer et al. (2001) for sediments from
294 this region, of 0.0048 to 0.006. Using $\text{Ba}/\text{Al}_{\text{detrital}} = 0.0055 \pm 0.0005$, the estimated
295 proportions of $\text{Ba}_{\text{excess}}$ range between 0 and 90% (Fig. 4c, Fig. 5, Supplementary Data
296 2).

297 There is a positive correlation between $\delta^{138/134}\text{Ba}$ values and $\text{Ba}_{\text{excess}}$, which
298 represents a mixing line between detrital and excess Ba, each featuring a distinct

299 isotope composition (Fig. 5). Through extrapolation, it can be inferred that excess Ba
300 exhibits slightly higher $\delta^{138/134}\text{Ba}$ values ($\approx +0.1$ ‰) than detrital Ba ($\delta^{138/134}\text{Ba} \approx -0.1$
301 to 0 ‰). The observed sediment $\delta^{138/134}\text{Ba}$ values do display subtle deviations from
302 this linear correlation that exceed analytical uncertainty. Without better constraints
303 however, it is not possible to ascertain whether these subtle variations are caused by
304 small variations in the isotope composition of excess Ba, or of detrital Ba or
305 $\text{Ba}/\text{Al}_{\text{detrital}}$ for individual samples. For example, sediments from station 18 exhibit
306 down core variations in $\text{Ba}_{\text{excess}}$ of approximately 60% to 10%, but display reasonable
307 constant $\delta^{138/134}\text{Ba}$ values of $+0.01 \pm 0.03$ ‰ (mean \pm 2SD; $n = 19$) (Fig. 4; Fig. 5;
308 Supplementary Data 2). This could indicate that both detrital and excess Ba have
309 similar $\delta^{138/134}\text{Ba}$ values at this site (of $\approx +0.01$ ‰), or that there are subtle down-core
310 variations in $\delta^{138/134}\text{Ba}$ values of one or both of these endmembers, coinciding with
311 the change in $\text{Ba}_{\text{excess}}$.

312 Difficulty in precisely calculating $\delta^{138/134}\text{Ba}$ values of excess Ba throughout
313 the sample set described above unfortunately precludes more detailed assessment of
314 the factors that could potentially cause subtle variations in the isotope composition of
315 excess Ba, both spatially across the sampled transect and within individual cores. For
316 example, isotopic variability in excess Ba due to diagenetic processes, or factors such
317 as water depth and barite saturation state of bottom waters, cannot be ruled out but
318 cannot be clearly resolved. In any case the total range of sediment Ba isotope
319 compositions are limited to 0.2 ‰, and the dominant control on the observed isotopic
320 variations is the proportion of $\text{Ba}_{\text{excess}}$ (Fig. 5). Therefore any potential variations in
321 the Ba isotope compositions of excess Ba in the sample set are likely to be less the 0.1
322 ‰. This discussion illustrates the challenge of accurately and precisely correcting Ba
323 excess $\delta^{138/134}\text{Ba}$ values for detrital Ba inputs. Studies attempting to discern subtle

324 isotopic variations in excess Ba will therefore need to carefully choose their sampling
325 sites to feature sediments with low detrital Ba contributions, which are typically found
326 in settings away from continental margins.

327 The inferred isotope composition of excess Ba is primarily constrained by
328 results for sediments from station 8, which feature particularly low detrital Ba
329 contributions (Fig. 5), and are characterized by $\delta^{138/134}\text{Ba} = +0.09 \pm 0.01 \text{ ‰}$ (mean \pm
330 2SE, n = 10). It is likely that BaSO_4 is the dominant phase hosting the excess Ba in
331 these sediments, but other phases such as carbonate minerals, organic matter or Fe-
332 Mn phases could also potentially be important (e.g. Eagle et al., 2003). Sediments
333 from station 8 are composed of 70 to 83 wt.% carbonate and 0 to 0.3 wt.% total
334 organic carbon (Supplementary Material; Supplementary Data 2). Following the
335 approach of Gingele & Dahmke (1994), and assuming this carbonate and organic
336 carbon have Ba concentrations of $30 \mu\text{g g}^{-1}$ and $60 \mu\text{g g}^{-1}$ respectively, we estimate
337 that these phases only contribute up to 5.7 % and 0.03 % of the excess Ba in these
338 sediments. This analysis supports the interpretation that the $\delta^{138/134}\text{Ba}$ values inferred
339 for excess Ba, of $+0.09 \pm 0.01 \text{ ‰}$, predominantly represents that of BaSO_4 , although
340 minor Ba contributions from Fe-Mn phases may also be possible. Regardless, the
341 $\delta^{138/134}\text{Ba}$ values of sediments from station 8 provide an important first constraint on
342 the isotope composition of Ba exported to the sediment through biogeochemical
343 processes occurring in the overlying water column.

344

345 *5.2 The Ba isotope systematics of seawater*

346

347 To understand the Ba isotope composition of sediments, particularly the
348 authigenic Ba, requires assessment of the controls on Ba isotope composition
349 imparted by processes in the overlying water column.

350 Depth profiles of Ba concentrations display quasi-nutrient type distributions
351 reflecting the net removal of Ba in the upper ocean, and a net regeneration at depth
352 (e.g. Jeandel et al., 1996; Fig. 2). Unlike true nutrient elements, however, Ba is not
353 quantitatively removed or regenerated during its vertical cycling, and is not known to
354 be actively taken up by marine phytoplankton (Paytan & Griffiths, 2007). The
355 precipitation of BaSO₄ in supersaturated micro-environments, coupled with the
356 subsequent dissolution of BaSO₄ particles in the under-saturated water column and at
357 the sediment-water interface, are thought to be the dominant processes controlling the
358 water-column distribution (e.g. Jeandel et al., 1996, Hoppema et al., 2010, Jacquet et
359 al., 2016). Passive removal by organic material and biogenic CaCO₃, as well as by
360 scavenging by Fe-Mn phases, may also influence the cycling of Ba in the ocean,
361 although the distribution and importance of such processes is poorly understood
362 (Dehairs et al., 1980, Dymond et al., 1992, Balakrishnan Nair et al., 2005, Sternberg
363 et al., 2005). Ocean circulation acts to redistribute and mix these signals, hence the
364 distribution of dissolved Ba in the ocean represents a combination of removal and
365 regeneration processes, interacting with water mixing and advection (e.g. Horner et
366 al., 2015, Bates et al., 2017, Hsieh & Henderson, 2017).

367 With the exception of the data presented by Cao et al. (2016) from the East
368 and South China Seas, previous studies found a strong co-variance between dissolved
369 Ba concentrations and isotope compositions at sites throughout the global ocean
370 (Horner et al., 2015, Bates et al. 2017, Hsieh & Henderson, 2017; Fig. 3). The results
371 obtained here are in good agreement with this relationship. Such a tight coupling

372 between dissolved Ba concentrations and $\delta^{138/134}\text{Ba}$ values requires that removal,
 373 regeneration and mixing processes all act to produce similar relationships between
 374 these parameters.

375 We apply simple models to consider the effects of Ba removal and
 376 regeneration processes, and water mass mixing on the observed Ba concentration-
 377 $\delta^{138/134}\text{Ba}$ systematics. Steady state fractionation models have previously been used to
 378 describe the partitioning of Ba between dissolved and particulate phases in the ocean
 379 with an associated isotope fractionation (Horner et al., 2015, Bates et al., 2017, Hsieh
 380 & Henderson, 2017), and the following equation has been widely used:

381

$$382 \quad \delta^{138/134}\text{Ba}_{\text{diss}} = \delta^{138/134}\text{Ba}_{\text{diss}, 0} + [1000 \times (\alpha_{\text{diss/part}} - 1)] \times (1 - f_{\text{diss}}) \quad (3)$$

383

384 where f_{diss} denotes the fraction of dissolved Ba remaining in seawater relative to the
 385 initial concentration, and $\delta^{138/134}\text{Ba}_{\text{diss}}$ and $\delta^{138/134}\text{Ba}_{\text{diss}, 0}$ denote current and the initial
 386 isotope composition of dissolved Ba, respectively. The isotope fractionation factor,
 387 $\alpha_{\text{diss/part}}$, is defined as the $^{138}\text{Ba}/^{134}\text{Ba}$ ratio of dissolved Ba ($_{\text{diss}}$), relative to the
 388 $^{138}\text{Ba}/^{134}\text{Ba}$ ratio of particulate Ba ($_{\text{part}}$).

389 The effect of Ba addition to deep waters by regeneration processes on
 390 dissolved Ba concentrations and $\delta^{138/134}\text{Ba}$ values in the water column can be
 391 calculated through isotopic mass balance (eqn. 4).

392

$$393 \quad \delta^{138/134}\text{Ba}_{\text{diss}} = (\delta^{138/134}\text{Ba}_{\text{pre}} \times f_{\text{pre}}) + (\delta^{138/134}\text{Ba}_{\text{regen}} \times f_{\text{regen}}) \quad (4)$$

394

395 Where $\delta^{138/134}\text{Ba}_{\text{pre}}$ and $\delta^{138/134}\text{Ba}_{\text{regen}}$ denote the isotope compositions of the
 396 ‘preformed’ Ba in the water, and the regenerated flux respectively, with f_{pre} and f_{regen}

397 representing the fraction of the Ba from the ‘preformed’ and ‘regenerated’ reservoirs
398 respectively (with $f_{\text{pre}} + f_{\text{regen}} = 1$). This equation simulates mixing between two Ba
399 endmembers - ‘preformed’ and ‘regenerated’ - that have fixed Ba isotope
400 compositions. If there is no isotope fractionation accompanying regeneration
401 processes, then the isotope composition of the regenerative flux is equivalent to those
402 of sinking particles.

403 Finally the mixing of two water masses featuring different Ba concentrations
404 and isotope compositions can be calculated as follows (eqn. 5).

405

$$406 \quad \delta^{138/134}\text{Ba}_{\text{diss}} = [(\delta_{,1} \times [\text{Ba}]_1 \times f_1) + (\delta_{,2} \times [\text{Ba}]_2 \times f_2)] / [([\text{Ba}]_1 \times f_1) + ([\text{Ba}]_2 \times f_2)] \quad (5)$$

407

408 where δ_1 and δ_2 represent the $\delta^{138/134}\text{Ba}$ values, $[\text{Ba}]_1$ and $[\text{Ba}]_2$ the Ba concentrations,
409 and f_1 and f_2 the fractional contributions of the two respective water masses (with $f_1 +$
410 $f_2 = 1$).

411 The observed correlation between Ba concentrations and $\delta^{138/134}\text{Ba}$ values in
412 the water column can be broadly reproduced by linear steady-state fractionation
413 models, as well as non-linear regeneration and water mass mixing models (Fig. 6; Fig.
414 7; Fig. 8). The relatively limited range of Ba concentrations throughout the water
415 column, of only about a factor of about 2 to 3, limits the curvature of water mass
416 mixing lines, and hence the possibility for mixing to significantly perturb
417 relationships between Ba concentrations and isotope compositions imparted by
418 biogeochemical processes (Fig. 6). Likewise, because Ba is not quantitatively
419 regenerated in the ocean interior, the observed Ba concentrations and $\delta^{138/134}\text{Ba}$ values
420 fall on sections of the regeneration curves that can broadly approximate the observed
421 linear relationship (Fig. 8). The similarity of trends produced by each of these types of

422 process, across the range of values observed in ocean waters, limits the potential for
423 coupled Ba concentration- $\delta^{138/134}\text{Ba}$ systematics to unravel the roles of these different
424 processes in setting the distribution of Ba in the ocean. The relatively simple Ba
425 concentration-isotope systematics should, however, be useful for understanding the
426 controls on the isotope compositions of particulate Ba exported to underlying
427 sediments.

428

429 *5.3 Constraining the fractionation factor associated with Ba removal from the ocean*

430

431 Constraining the magnitude of the isotope fractionation accompanying Ba
432 removal processes is crucial for understanding Ba isotope cycling in the ocean.
433 Previous studies fit steady state fractionation models to the observed correlation
434 between dissolved Ba concentrations and $\delta^{138/134}\text{Ba}$ values to derive fractionation
435 factors, $\alpha_{\text{diss/part}}$ ranging from 1.00028 to 1.00058 (eqn. 3; Horner et al., 2015, Bates et
436 al., 2017, Hsieh & Henderson, 2017). This approach is subject to uncertainty in the
437 choice of the appropriate initial Ba concentration and $\delta^{138/134}\text{Ba}$ value (eqn. 3). This
438 uncertainty is driven by a lack of understanding of how much of the observed
439 variance in water column Ba concentrations and $\delta^{138/134}\text{Ba}$ values are controlled by
440 removal versus regeneration and mixing processes. For example, Horner et al. (2015)
441 and Bates et al. (2017) made the assumption that the distribution of dissolved Ba in
442 the upper 1000 m to 600 m of the water column is predominantly due to variable
443 degrees of Ba removal to particulate phases, to derive estimates of $\alpha_{\text{diss/part}}$ between
444 1.00028 and 1.00045. In contrast, Hsieh & Henderson (2017) assumed initial Ba
445 concentrations and $\delta^{138/134}\text{Ba}$ of $99.7 \text{ nmol kg}^{-1}$ and $+0.25 \text{ ‰}$ from waters upwelled in
446 the Southern Ocean to derive a maximum estimated $\alpha_{\text{diss/part}}$ of 1.00058 ± 10 .

447 We first follow these previous approaches, but with the addition of the new
448 data of this study to literature data (Horner et al., 2015, Bates et al., 2017, Hsieh &
449 Henderson, 2017). Fractionation factors ($\alpha_{\text{diss/part}}$) are calculated by fitting
450 fractionation models (eqn. 3) to linear regressions of the dissolved Ba concentrations
451 and $\delta^{138/134}\text{Ba}$ values, with uncertainty assessed by the 95% confidence interval of the
452 regression coefficient (Fig. 7). Taking a similar approach to Horner et al. (2015) and
453 Bates et al. (2017), and using initial concentrations and isotope compositions of 60
454 nmol kg^{-1} and +0.47 ‰, yields an $\alpha_{\text{diss/part}}$ of 1.00035 ± 6 (Fig. 7a). Following a
455 similar approach to Hsieh and Henderson (2017), using initial concentrations and
456 isotope compositions of 100 nmol kg^{-1} and +0.25 ‰, a larger $\alpha_{\text{diss/part}}$ of 1.00052 ± 3 is
457 obtained (Fig. 7b).

458 Alternative constraints on the magnitude of the isotope fractionation
459 accompanying Ba removal from seawater can be obtained by comparing the
460 difference in isotope composition of sinking particulate Ba to that of the waters from
461 which this Ba is derived. The Ba isotope composition inferred for sedimentary excess
462 Ba of $\delta^{138/134}\text{Ba} = +0.09 \pm 0.01$ ‰ (mean \pm 2SE, $n = 10$) presumably represents that of
463 accumulated sinking particles. As validation of this assumption, isotopic mass balance
464 models simulating the regeneration of particulate Ba (eqn. 4) can reproduce the
465 observed relationship between dissolved Ba concentrations and isotope compositions
466 with regenerative fluxes characterized by $\delta^{138/134}\text{Ba} = 0$ to +0.1 ‰ (Fig. 8). If there is
467 no significant isotope fractionation accompanying Ba regeneration, which is likely in
468 the case of BaSO_4 dissolution (von Allmen et al., 2010), these compositions provide
469 an assessment of the globally averaged $\delta^{138/134}\text{Ba}$ values of sinking particulate Ba.
470 These models assume the endmember scenario in which increases in dissolved Ba
471 concentrations with depth, and associated decreases in $\delta^{138/134}\text{Ba}$ values are purely

472 controlled by the addition of Ba from sinking particles. This is of course an
473 oversimplification, and there is uncertainty in the appropriate choice of ‘preformed’
474 Ba concentrations and $\delta^{138/134}\text{Ba}$ values. However, varying the ‘preformed’
475 compositions from those of South Atlantic surface waters ($\delta^{138/134}\text{Ba} = +0.6 \text{ ‰}$; Fig.
476 8a), to those of deeper waters (e.g. $\delta^{138/134}\text{Ba} = +0.45 \text{ ‰}$; Fig. 8b), makes only
477 marginal differences in the predicted regenerative flux compositions.

478 The depth range over which Ba is removed from seawater to sinking particles
479 will influence the estimated isotope fractionation because dissolved $\delta^{138/134}\text{Ba}$ values
480 vary over the upper 1000 m of the water column (Fig. 2). The precipitation of BaSO_4 ,
481 the dominant oceanic sink of Ba, is likely to predominantly occur in the upper 500 m
482 of the water column based on typical depths of maxima in concentrations of
483 suspended particulate Ba (e.g. Cardinal et al., 2005, Sternberg et al., 2008, Planchon
484 et al., 2013, Jacquet et al., 2015).

485 Assuming the vast majority of sinking particulate Ba, characterized by
486 $\delta^{138/134}\text{Ba} \approx +0.1 \text{ ‰}$, is formed in the upper 500 m of the water column, characterized
487 by $\delta^{138/134}\text{Ba} \approx +0.5$ to $+0.6 \text{ ‰}$, corresponds to an isotope fractionation of
488 $\Delta^{138/134}\text{Ba}_{\text{diss-part}} = +0.4$ to $+0.5$ (or $\alpha_{\text{diss/part}} = 1.0004$ to 1.0005 ; where $\Delta^{138/134}\text{Ba}_{\text{diss-part}}$
489 $= 1000 \times (\alpha_{\text{diss/part}} - 1)$). These values represent maximum estimates because sinking
490 particulate Ba could also be removed from seawater below the specified depth, in
491 which case it would be derived from a dissolved Ba reservoir with lower $\delta^{138/134}\text{Ba}$
492 values (Fig. 2). For instance, evidence from sediment trap fluxes and Ra isotopes
493 suggesting significant components of the Ba sinking flux can be derived from several
494 1000 m in the water column (Dymond et al., 1992, Dymond & Collier, 1996, Dehairs
495 et al., 2000, McManus et al., 2002, van Beek et al., 2007, 2009). The importance of
496 Ba removal from deeper in the water column is, however, poorly known. Ultimately

497 the determination of suspended particulate Ba isotope compositions, particularly in
498 the upper few hundred meters of the water column where dissolved $\delta^{138/134}\text{Ba}$ values
499 are constant, will lead to more precise constraints. This in turn could help to better
500 constrain the depth range over which Ba removal from the water column occurs.

501

502 *5.4 Controls on the isotope composition of sedimentary excess Ba*

503

504 The observed relationship between Ba concentration and isotope composition
505 in the water column imply that the isotope fractionation associated with Ba removal
506 must be reasonably constant throughout the ocean (Fig. 3). By assuming that the
507 majority of excess Ba is removed from the upper 500 m of the water column, we
508 estimate the magnitude of this isotopic fractionation to be $\Delta^{138/134}\text{Ba}_{\text{diss-part}} = +0.4$ to
509 $+0.5$ (section 5.3). Taken together, we hypothesize that the isotope composition of
510 excess Ba accumulating in marine sediments depends directly on the isotope
511 composition of the dissolved Ba in upper ocean waters from which it is derived. This
512 hypothesis can be confirmed by measurement of the isotope composition of
513 sedimentary excess Ba across the gradients in upper ocean dissolved Ba
514 concentrations and $\delta^{138/134}\text{Ba}$ values.

515 Barium isotope compositions of open ocean sediments could therefore record
516 changes in the balance between the supply and removal of Ba from upper ocean
517 waters, which in turn could provide constraints on export production in the past.
518 Specifically, increased Ba supply through upwelling or external riverine inputs would
519 act to decrease $\delta^{138/134}\text{Ba}$ values (Hsieh & Henderson, 2017), whereas increased Ba
520 removal, related to export production, would act to increase $\delta^{138/134}\text{Ba}$ values. Upper
521 ocean Ba concentrations are relatively homogeneous over large spatial scales due to

522 the importance of horizontal mixing (Hsieh & Henderson, 2017). Therefore, the
523 dissolved Ba content of upper ocean waters, and hence Ba isotope compositions of
524 sedimentary excess Ba, are unlikely to be significantly influenced by local
525 biogeochemical processes, but rather record processes integrated over a broad basin
526 scale (Hsieh & Henderson, 2017).

527 A particular advantage of Ba isotope composition variations for recording past
528 perturbations to upper ocean Ba cycling, related to export production, is that they
529 should be unaffected by uncertainty in BaSO₄ preservation rates and sediment mass
530 accumulation rate estimates. Insights provided by Ba isotope composition variations
531 of sedimentary excess Ba could therefore improve the application of Ba accumulation
532 rates in sediments as a proxy for export production during periods of climatic change.
533 For example, the recovery from the Paleocene-Eocene Thermal Maximum is marked
534 by increases in Ba concentrations in open ocean marine sediments, which has been
535 cited as evidence for the role of export production for the sequestration of carbon
536 from the atmosphere-ocean system (Bains et al., 2000, Ma et al., 2014). There is
537 however disagreement in sedimentation rates across these sedimentary sections,
538 which imparts significant uncertainty into reconstructions of Ba accumulation rates,
539 and thus both the timing and magnitude of changes in export production at this time
540 period (Torfstein et al., 2010). The application of Ba isotope variations to such
541 sediments may provide useful insights into perturbations to upper ocean Ba cycling
542 necessary for the robust application of the Ba proxy for export production.

543

544 **6. Conclusions**

545

546 First constraints on the Ba isotope compositions of marine sediments are
547 presented for samples collected along a transect extending from the Uruguayan
548 continental margin to the mid Atlantic Ridge. The dominant control on the observed
549 variations in Ba isotope compositions of these samples is mixing between detrital and
550 authigenic Ba (excess Ba). These two sedimentary Ba sources exhibit rather similar
551 isotope compositions, which will make the determination of sedimentary excess Ba
552 isotope compositions challenging in environments that receive high inputs of detrital
553 Ba. Open ocean sediments constrain the isotope composition of excess Ba to be
554 $\delta^{138/134}\text{Ba} = +0.09 \pm 0.01 \text{ ‰}$ (mean \pm 2SE, n = 10). This is similar to that inferred for
555 globally averaged sinking particulate Ba fluxes.

556 The relatively simple Ba concentration-isotope composition systematics of
557 dissolved Ba in the water column suggests that the magnitude of the isotope
558 fractionation accompanying removal processes is reasonable constant throughout the
559 ocean, which is likely to be in the range +0.4 to +0.5 ‰. The isotope composition of
560 sedimentary excess Ba is therefore hypothesized to record those of the overlying
561 upper water column. The implications are that $\delta^{138/134}\text{Ba}$ values of sedimentary excess
562 Ba may allow reconstruction of past perturbations in cycling of Ba in the upper ocean.
563 In particular, changes in Ba removal rates (related to export production) and Ba
564 supply rates (related to upwelling and possibly riverine inputs) to the upper water
565 column should influence dissolved Ba isotope compositions, and this variation will
566 likely be recorded by sedimentary Ba isotope signatures. Such insights should be
567 insensitive to uncertainties in BaSO_4 preservation and sedimentation rates, and thus
568 help better constrain the use of Ba in marine sediments as a paleo-proxy for export
569 production.

570

571 **Acknowledgements**

572 We thank the captain, crew and science party of the *RRS James Cook* during the
573 JC068 expedition. We also thank Phil Holdship for his role in conducting
574 measurements of Ba and Al concentrations of sediment samples by ICP-MS, Freya
575 Hemsing for assistance refining analytical techniques and providing Ba isotope
576 measurements of standard reference materials, and Malcolm Woodward who
577 performed shipboard analyses of nitrate in porewater samples. Funding for this work
578 was in part provided by Shell Global Solutions BV. Rachel Mills (University of
579 Southampton) supported WBH for the collection of sediments and porewater and
580 analyses of oxygen, metals and carbon through NERC grants (NE/F017197/1 and
581 NE/H004394/1). WBH was also supported by a NERC fellowship (NE/K009532/1).
582 Tristan Horner, Damien Cardinal and an anonymous reviewer are thanked for their
583 constructive comments, which helped to improve this manuscript.

584

585 **References**

- 586 Anderson, R. F. & Winckler, G., 2005, Problems with paleoproductivity proxies,
587 *Paleoceanography*, 20, 3012, doi:10.1029/2004PA001107
- 588
- 589 Bains, S., Norris, R. D., Corfield, R. M. & Faul, K. L., 2000, Termination of global
590 warmth at the Paleocene/Eocene boundary through productivity feedback, *Nature*,
591 407, 171-174
- 592
- 593 Balakrishnan Nair, T. M., Ittekkot, V., Shankar, R. & Guptha, M. V. S., 2005, Settling
594 barium fluxes in the Arabian Sea: Critical evaluation of relationship with export
595 production, *Deep-Sea Research II*, 52, 1930-1946, doi:10.1016/j.dsr2.2005.06.003

596

597 Bates, S. L., Hendry, K. R., Pryer, H. V., Kinsley, C. W., Pyle, K. M., Woodward, E.
598 M. S. & Horner, T. J., 2017, Barium isotopes reveal role of ocean circulation on
599 barium cycling in the Atlantic, *Geochimica et Cosmochimica Acta*, 204, 286-299,
600 doi:10.1016/j.gca.2017.01.043

601

602 Bernstein, R. E. & Byrne, R. H., 2004, Acantharians and marine barite, *Marine*
603 *Chemistry*, 86, 45-50, doi:10.1016/j.marchem.2003.12.003

604

605 Bishop, J. K. B., 1988, The barite-opal-organic carbon association in oceanic
606 particulate matter, *Nature*, 322, 341-343

607

608 Cao, Z., Siebert, C., Hathorne, E. C., Dai, M. & Frank, M., 2016, Constraining the
609 oceanic barium cycle with stable barium isotopes, *Earth and Planetary Science*
610 *Letters*, 434, 1-9, doi:10.1016/j.epsl.2015.11.017

611

612 Cardinal, D., Savoye, N., Trull, T. W., André, L., Kopczynska, E., & Dehairs, F.,
613 2005, Variations of carbon remineralisation in the Southern Ocean illustrated by the
614 Ba_{xs} proxy, *Deep-Sea Research I*, 52, 355-370, doi:10.1016/j.dsr.2004.10.002

615

616 Dehairs, F., Chesselet, R., & Jebwab, J., 1980, Discrete suspended particles of barite
617 and the barium cycle in the open ocean, *Earth and Planetary Science Letters*, 49, 528-
618 550

619

620 Dehairs, F., Fagel, N., Antia, A. N., Peinert, R., Elskens, M. & Goeyens, L., 2000,
621 Export production in the Bay of Biscay as estimated from barium – barite in settling
622 material: a comparison with new production, *Deep-Sea Research I*, 47, 583-601
623

624 Dickens, G., Fewless, E., Thomas, E. & Bralower, T., 2003, Excess barite
625 accumulation during the Paleocene/Eocene thermal maximum: Massive input of
626 dissolved barium from seafloor gas hydrate reservoirs, *in* Ginerich, P., et al., eds.,
627 Causes and consequences of globally warm climates in the early Paleogene:
628 Geological Society of America Special Paper 369, p. 11-23
629

630 Dymond, J., Suess, E. & Lyle, E., 1992, Barium in deep-sea sediment: A geochemical
631 proxy for paleoproductivity, *Paleoceanography*, 7 (2), 163-181
632

633 Dymond, J. & Collier, R., 1996, Particulate barium fluxes and their relationships to
634 biological productivity, *Deep-Sea Research II*, 43, 1283-1308
635

636 Eagle, M., Paytan, A., Arrigo, K. R., van Dijken, G. & Murray, R. W., 2003, A
637 comparison between excess barium and barite as indicators of carbon export,
638 *Paleoceanography*, 18, 1, 1021, doi:10.1029/2002PA000793
639

640 Fagel, N., Dehairs, F., Andre, L., Bareille, G. & Monnin, C., 2002, Ba distribution in
641 surface Southern Ocean sediments and export production estimates,
642 *Paleoceanography*, 17 (2), 1011, doi:10.1029/2000PA000552
643

644 Foster, D. A., Staubwasser, M. & Henderson, G. M., 2004, ^{226}Ra and Ba
645 concentrations in the Ross Sea measured with multicollector ICP mass spectrometry,
646 *Marine Chemistry*, 87, 59-71, doi:10.1016/j.marchem.2004.02.003
647
648 Francois, R., Honjo, S., Manganini, S. J. & Ravizza, G. E., 1995, Biogenic barium
649 fluxes to the deep sea: Implications for paleoproductivity reconstruction, *Global*
650 *Biogeochemical Cycles*, 9 (2) 289-303
651
652 Ganeshram R. S., François, R., Commeau, J. & Brown-Leger, S. L., 2003, An
653 experimental investigation of barite formation in seawater, *Geochimica et*
654 *Cosmochimica Acta*, 67 (14), 2599-2605
655
656 Gingele, F. & Dahmke, A., 1994, Discrete barite particles and barium as tracers of
657 paleoproductivity in South Atlantic sediments, *Paleoceanography*, 9 (1), 151-168
658
659 Homoky, W.B., Hembury, D.J., Hepburn, L.E., Mills, R.A., Statham P.J., Fones, G. &
660 Palmer, M. 2011 Iron and Manganese diagenesis in deep sea volcanogenic sediments
661 and the origins of pore water colloids. . *Geochim. Cosmochim. Acta* 75, 5032-5048.
662
663 Homoky, W. B., John, S. G., Conway, T. M. & Mills, R. A., 2013, Distinct iron
664 isotopic signatures and supply from marine sediment dissolution, *Nature*
665 *Communications*, 4, 2143, doi:10.1038/ncomms3143
666
667 Hoppema, M., Dehairs, F., Navez, J., Monnin, C., Jeandel, C., Fahrbach, E. & de
668 Baar, H. J. W., 2010, Distribution of barium in the Weddell Gyre: Impact of

669 circulation and biogeochemical processes, *Marine Chemistry*, 122, 118-129,
670 doi:10.1016/j.marchem.2010.07.005
671
672 Horner, T. J., Kinsley, C. W. & Nielsen, S. G, 2015, Barium isotope fractionation in
673 seawater mediated by barite cycling and oceanic circulation, *Earth and Planetary*
674 *Science Letters*, 430, 511-522, doi:10.1016/j.epsl,2015.07.027
675
676 Hsieh, Y-T. & Henderson, G. M., 2017, Barium stable isotopes in the global ocean:
677 Tracer of Ba utilization and inputs, *Earth and Planetary Science Letters*, 473, 269-
678 278, doi.org/10.1016/j.epsl.2017.06.024
679
680 Jacquet, S. H. M., Dehairs, F., Lefevre, D., Cavagna, A. J., Planchon, F., Christaki,
681 U., Monin, L., André, L., Closset, I. & Cardinal, D, 2015, Early spring mesopelagic
682 carbon remineralization and transfer efficiency in the naturally iron-fertilized
683 Kerguelen area, *Biogeosciences*, 12, 1713-1731, doi:10.5194/bg-12-1713-2015
684
685 Jacquet, S. H. M., Monnin, C., Riou, V., Jullion, L. & Tanhua, T., 2016, A high
686 resolution and quasi-zonal transect of dissolved Ba in the Mediterranean Sea, *Marine*
687 *Chemistry*, 178, 1-7, doi:10.1016/j.marchem.2015.12.001
688
689 Jeandel, C., Dupré, B., Lebaron, G., Monnin, C. & Minster, J. F., 1996, Longitudinal
690 distributions of dissolved barium, silica and alkalinity in the western and southern
691 Indian Ocean, *Deep-Sea Research I*, 43 (1), 1-31
692

693 Klump, J., Hebbeln, D. & Wefer, G., 2000, The impact of sediment provenance on
694 barium-based productivity estimates, *Marine Geology*, 169, 259-271
695
696 Legeleux, F. & Reyss, J-L, 1996, $^{228}\text{Ra}/^{226}\text{Ra}$ activity ratio in oceanic settling
697 particles: implications regarding the use of barium as a proxy for paleoproductivity
698 reconstruction, *Deep-Sea Research I*, 45 (11-12), 1857-1863
699
700 Mawji et al., 2015, The GEOTRACES intermediate data product 2014, *Marine*
701 *Chemistry*, 177 (1), 1-8, doi:10.1016/j.marchem.2015.04.005
702
703 Ma, Z., Gray, E., Thomas, E., Murphy, B., Zachos, J. & Paytan, A., 2014, Carbon
704 sequestration during the Palaeocene-Eocene Thermal Maximum by an efficient
705 biological pump, *Nature Geoscience*, 7, 382-388, doi:10.1038/NGEO2139
706
707 McManus, J., Dymond, J., Dunbar, R. B. & Collier, R. W, 2002, Particulate barium
708 fluxes in the Ross Sea, *Marine Geology*, 184, 1-15
709
710 Monnin, C., Jeandel, C., Cattaldo, T, & Dehairs, F., 1999, The marine barite
711 saturation state of the world's oceans, *Marine Chemistry*, 65, 253-261
712
713 Nan, X., Wu, F., Zhang, Z., Hou, Z., Huang, F, & Yu, H., 2015, High-precision
714 barium isotope measurements by MC-ICP-MS, *Journal of Analytical Atomic*
715 *Spectrometry*, doi:10.1039/c5ja00166h
716

717 Paytan, A., & Griffiths, E. M., 2007, Marine barite: Recorder of variations in ocean
718 export productivity, *Deep-Sea Research II*, 54, 687-705,
719 doi:10.1016/j.dsr2.2007.01.007
720

721 Paytan, A & Kastner, M., 1996, Benthic Ba fluxes in the central Equatorial Pacific,
722 implications for the oceanic Ba cycle, *Earth and Planetary Science Letters*, 142, 439-
723 450
724

725 Pfeifer, K., Kasten, S., Hensen, C. & Schulz, H. D., 2001, Reconstruction of primary
726 productivity from the barium contents in surface sediments of the South Atlantic
727 Ocean, *Marine Geology*, 177, 13-14
728

729 Planchon, F., Cavagna, A.-J., Cardinal, D., André, L. & Dehairs, F., 2013, Late
730 summer particulate organic carbon export and twilight zone remineralisation in the
731 Atlantic sector of the Southern Ocean, *Biogeosciences*, 10, 8030820, doi:10.5194/bg-
732 10-803-2013
733

734 Reitz, A., Pfeifer, K., de Lange, G. J. & Klump, J., 2004, Biogenic barium and the
735 detrital Ba/Al ratio: a comparison of their direct and indirect determination, *Marine*
736 *Geology*, 204, 289-300, doi:10.1016/S0025-3227(04)00004-0
737

738 Schlitzer, R., (2015), Ocean Data View, <http://odv.awi.de>
739

740 Sternberg, E., Jeandel, C, Miquel, J. C., Gasser, B, Souhaut, M, Arraes-Mescoff, R. &
741 Francois, R., 2007, Particulate barium fluxes and export production in the

742 northwestern Mediterranean, *Marine Chemistry*, 105, 281-295,
743 doi:10.1016/j.marchem.2007.03.003
744
745 Sternberg, E., Jeandel, C, Robin, E., & Souhaut, M., 2008, Seasonal cycle of
746 suspended barite in the mediterranean sea, , *Geochimica et Cosmochimica Acta*, 72,
747 4020-4034, doi:10.1016/j.gca.2008.05.043
748
749 Sternberg, E., Tang, D., Ho, T-Y., Jeandel, C. & Morel, F. M. M., 2005, Barium
750 uptake and adsorption in diatoms, *Geochimica et Cosmochimica Acta*, 69, 2745-2752
751
752 Torres, M. E., Brumsack, H. J., Bohrmann, G. & Emeis, K. C., 1996, Barite fronts in
753 continental margin sediments: A new look at barium remobilization in the zone of
754 sulfate reduction and formation of heavy barites in diagenetic fronts, *Chemical*
755 *Geology*, 127, 125-139
756
757 Torfstein, A., Winckler, G. & Tripathi, A., 2010, Productivity feedback did not
758 terminate the Paleocene-Eocene Thermal Maximum (PETM), *Climate of the Past*, 6,
759 265-272
760
761 van Beek, P., François, R., Conte, M., Reyss, J-L., Souhaut, M. & Charette, M., 2007,
762 $^{228}\text{Ra}/^{226}\text{Ra}$ and $^{226}\text{Ra}/\text{Ba}$ ratios to track barite formation and transport in the water
763 column, *Geochimica et Cosmochimica Acta*, 71, 71-86,
764 doi:10.1016/j.gca.2006.07.041
765

766 van Beek, P., Sternberg, E., Reyss, J-L., Souhaut, M., Robin, E. & Jeandel, C., 2009,
767 $^{228}\text{Ra}/^{226}\text{Ra}$ and $^{226}\text{Ra}/\text{Ba}$ ratios in the Western Mediterranean Sea: Barite formation
768 and transport, *Geochimica et Cosmochimica Acta*, 73, 4720-4737,
769 doi:10.1016/j.gca.2009.05.063

770

771 von Allmen, K., Böttcher, M. E., Samankassou, E., Nägler, T. F., 2010, Barium
772 isotope fractionation in the global barium cycle: First evidence from barium minerals
773 and precipitation experiments, *Chemical Geology*, 277, 70-77,
774 doi:10.1016/j.chemgeo.2010.07.011

775

776 Wyatt, N. J., Milne, A., Woodward, E. M. S., Rees, A. P., Browning, T. J., Bouman,
777 H. A., Worsfold, P. J. & Lohan, M. C., 2014, Biogeochemical cycling of dissolved
778 zinc along the GEOTRACES South Atlantic transect GA10 at 40°S, *Global*
779 *Biogeochemical Cycles*, 28, 44-56, doi:10.1002/2013GB004637

780

781 **Figure 1;** Sampling locations for seawater depth profiles and sediment cores. Panel
782 (a) shows map of station (stn) locations for collection of seawater depth profiles
783 (circles) and sediment cores (squares). Note that the results for the seawater depth
784 profile at station 20 have been previously published (Hsieh & Henderson, 2017).
785 Panel (b) displays a vertical section of salinity along the GEOTRACES GA10 section,
786 with sampling locations. The main water masses are labeled; AAIW – Antarctic
787 Intermediate Water, UCDW – Upper Circumpolar Deep Water, NADW – North
788 Atlantic Deep Water, AABW – Antarctic Bottom Water. Also shown is the location
789 of seawater depth profiles for Ba concentrations and isotope compositions published

790 by Horner et al. (2015), at station 6, and Bates et al. (2017), at station 3. Figure
791 produced using Ocean Data View (Schlitzer, 2015).

792

793 **Figure 2;** Seawater depth profiles of dissolved Ba concentrations (open circles) and
794 $\delta^{138/134}\text{Ba}$ values (closed circles). Panels (a) to (e) display results for the upper 1000 m
795 of the water column on an expanded scale, while panels (f) to (i) display results for
796 the full range of depths. Note that results for station 22 only extend down to 996 m.
797 Results for station 20 have been previously presented by Hsieh & Henderson (2017).
798

799 **Figure 3;** Relationship between dissolved Ba concentrations and $\delta^{138/134}\text{Ba}$ values for
800 seawater samples. Displayed are results from the South Atlantic (this study, Horner et
801 al., 2015, Bates et al., 2017, Hsieh & Henderson, 2017), as well as literature values
802 for the North Atlantic, Southern Ocean and North Pacific (Bates et al., 2017, Hsieh &
803 Henderson, 2017), which display a consistent relationship. Note that results published
804 by Cao et al. (2016) have been excluded from the compilation as they exhibit a
805 different relationship between these parameters, with higher $\delta^{138/134}\text{Ba}$ values.

806

807 **Figure 4;** Elemental and Ba isotope composition results for the sediment cores as a
808 function of depth below seafloor. The proportions of non-detrital Ba ($\text{Ba}_{\text{excess}}$) are
809 estimated assuming a detrital Ba/Al ratio of 0.0055 ± 0.0005 .

810

811 **Figure 5;** The relationship between estimated proportions non-detrital Ba ($\text{Ba}_{\text{excess}}$)
812 versus $\delta^{138/134}\text{Ba}$ values for the sediment samples. The fractional contributions of
813 excess Ba are calculated assuming a detrital Ba/Al ratio of 0.0055 ± 0.0005 .

814

815 **Figure 6;** Bimodal mixing trends between waters with different Ba concentrations
816 and $\delta^{138/134}\text{Ba}$ values, spanning the observed range of values in the water column. The
817 light grey, dark grey and black lines show mixing between South Atlantic surface
818 waters (40 nmol kg⁻¹, and $\delta^{138/134}\text{Ba} = +0.6$ ‰), and waters with 50 nmol kg⁻¹/
819 $\delta^{138/134}\text{Ba} = +0.5$ ‰, 70 nmol kg⁻¹/ $\delta^{138/134}\text{Ba} = +0.37$ ‰ and 100 nmol kg⁻¹/ $\delta^{138/134}\text{Ba}$
820 = +0.25 ‰ respectively. The chosen endmembers are not intended to reproduce any
821 specific mixing scenarios expected to be important, only to demonstrate a range of
822 theoretically possible mixing relationships. Note that the degree of curvature of the
823 mixing trends decreases with decreasing difference in Ba concentrations of the two
824 water masses (eqn. 5). Literature dissolved Ba concentration and isotope composition
825 data are from Horner et al. (2015), Bates et al., (2017) and Hsieh & Henderson
826 (2017).

827

828 **Figure 7;** Isotope fractionation models explaining the observed relationship between
829 dissolved Ba concentrations and isotope compositions in the water column. Panels (a)
830 and (b) display steady state fractionation models assuming Ba removal from waters
831 with an initial Ba concentrations of 60 nmol kg⁻¹ and 100 nmol kg⁻¹ respectively (i.e.
832 following the approaches of Bates et al. (2017) and Hsieh and Henderson (2017)
833 respectively; see section 5.3). Fractionation factors ($\alpha_{\text{diss/part}}$) are derived by fitting
834 fractionation models (eqn. 3) to linear regressions of the data, with uncertainty
835 assessed using the 95% confidence interval of the regression coefficient (dashed
836 lines). The predicted isotope compositions of resulting particulate phases are
837 constrained by the fractionation factor. The isotope composition of sedimentary
838 excess Ba, defined by sediments of station 8 (e.g. Fig 5) is shown as a brown line for
839 reference. The grey shaded areas highlight the isotope composition of particulate Ba

840 predicted to form from waters in the upper 500 m featuring $\delta^{138/134}\text{Ba} = +0.5$ to $+0.6$
841 ‰. Approximate water depths corresponding to the dissolved Ba concentrations and
842 $\delta^{138/134}\text{Ba}$ values for Atlantic data are labeled. Literature dissolved Ba concentration
843 and isotope composition data are from Horner et al. (2015), Bates et al., (2017) and
844 Hsieh & Henderson (2017).

845

846 **Figure 8;** Isotope mass balance models explaining the observed variance in dissolved
847 Ba concentrations and isotope compositions in terms of the addition of Ba through the
848 regeneration of sinking particulate Ba. Panels (a) and (b) display regeneration models
849 assuming a pre-formed Ba concentration and $\delta^{138/134}\text{Ba}$ value of 40 nmol kg^{-1} and $+0.6$
850 ‰ and 60 nmol kg^{-1} and $+0.45$ ‰ respectively (eqn. 4), and are intended to illustrate
851 the effect of varying the pre-formed endmember on the model calculations. For each
852 model, the isotope composition of the regenerated particulate Ba is labeled. Literature
853 dissolved Ba concentration and isotope composition data are from Horner et al.
854 (2015), Bates et al., (2017) and Hsieh & Henderson (2017).

855

856

857

858

859

860

861

862

863

864

Figure 1

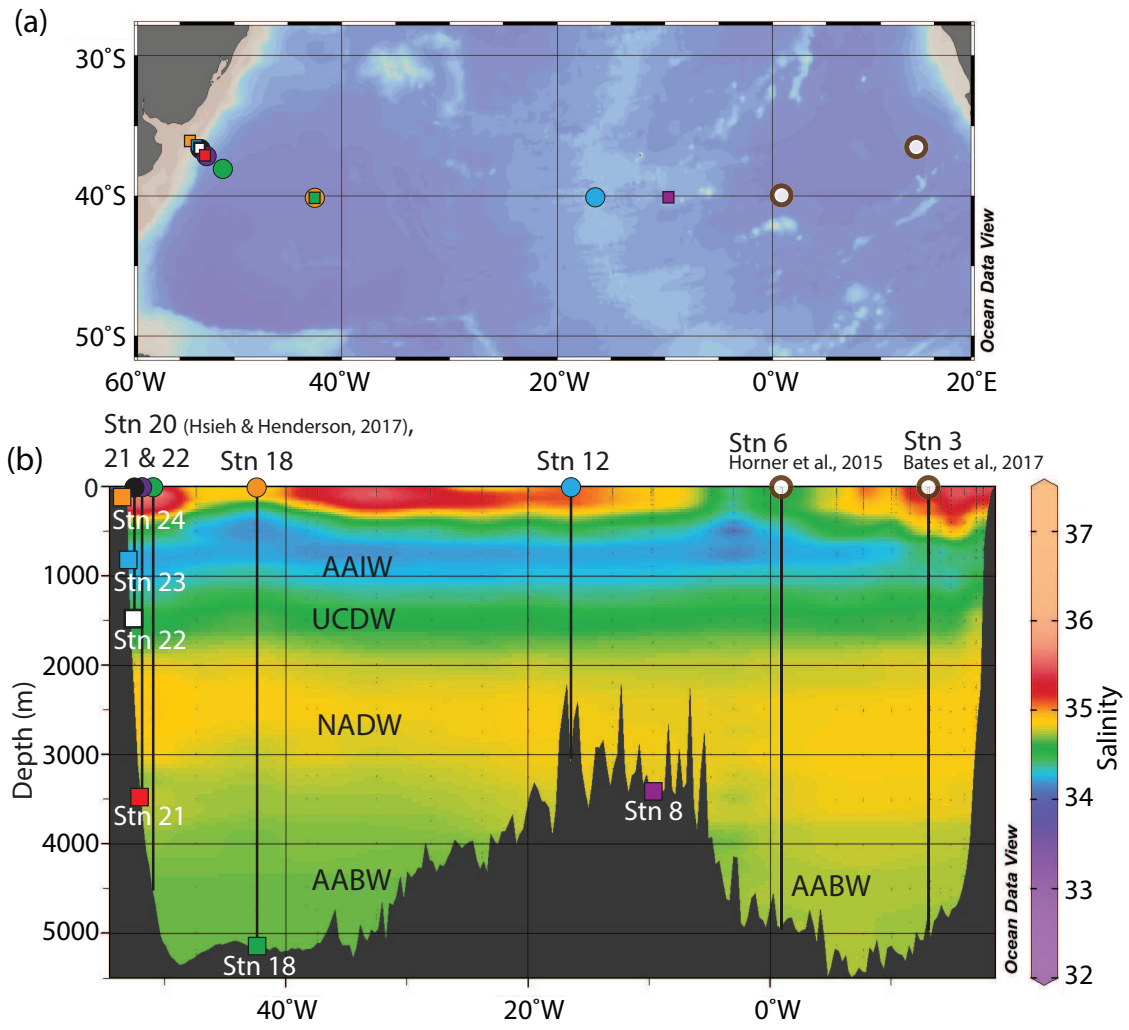


Figure 2

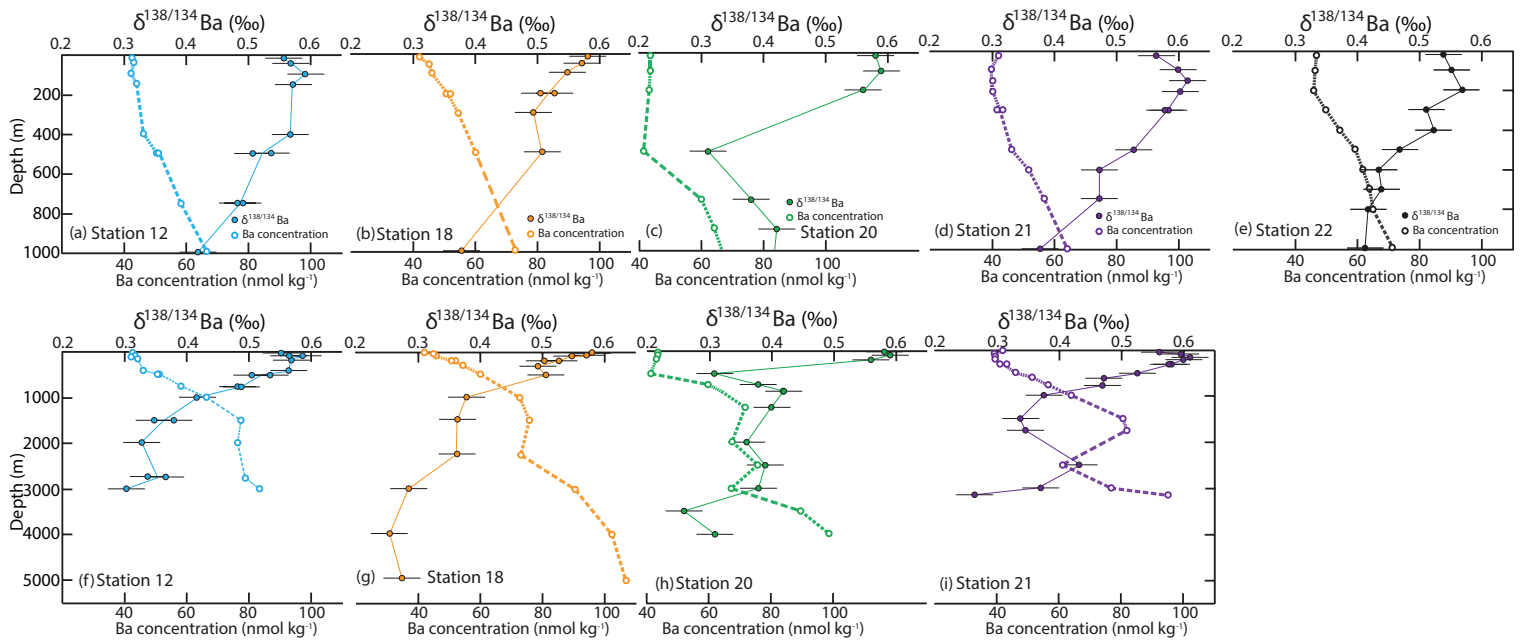


Figure 3

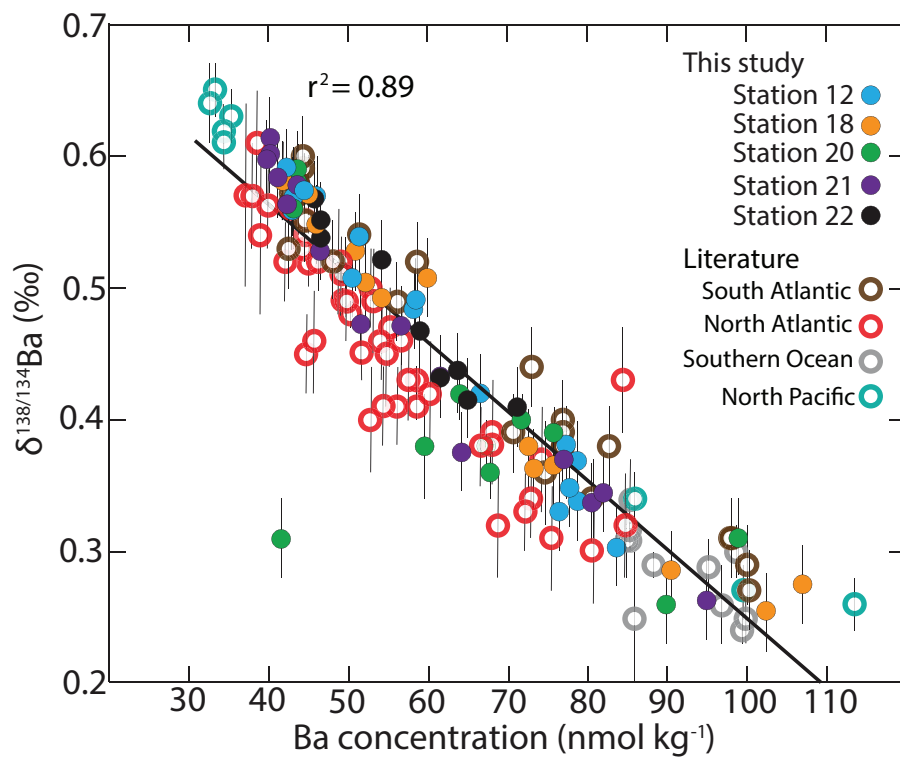


Figure 4

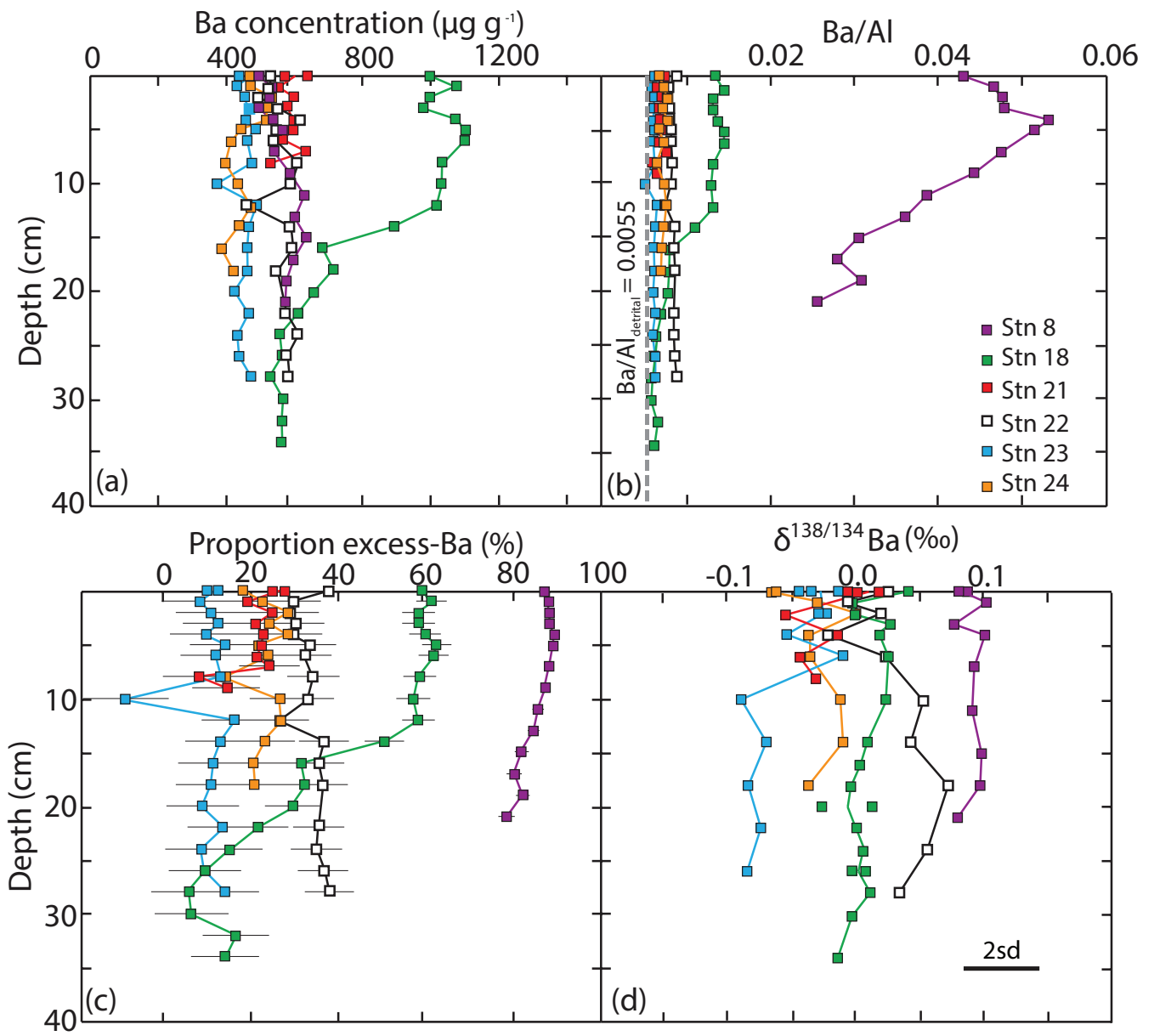


Figure 5

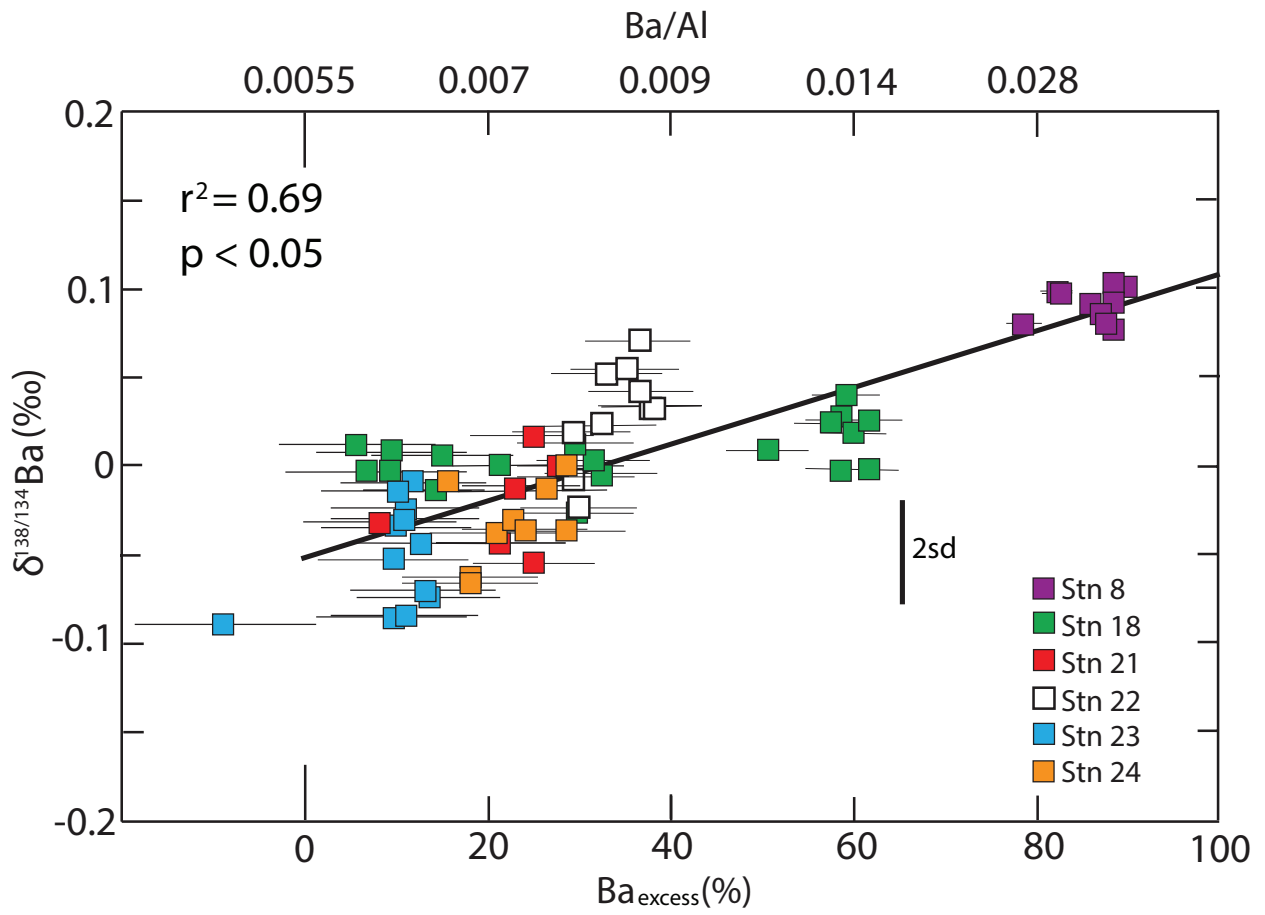


Figure 6

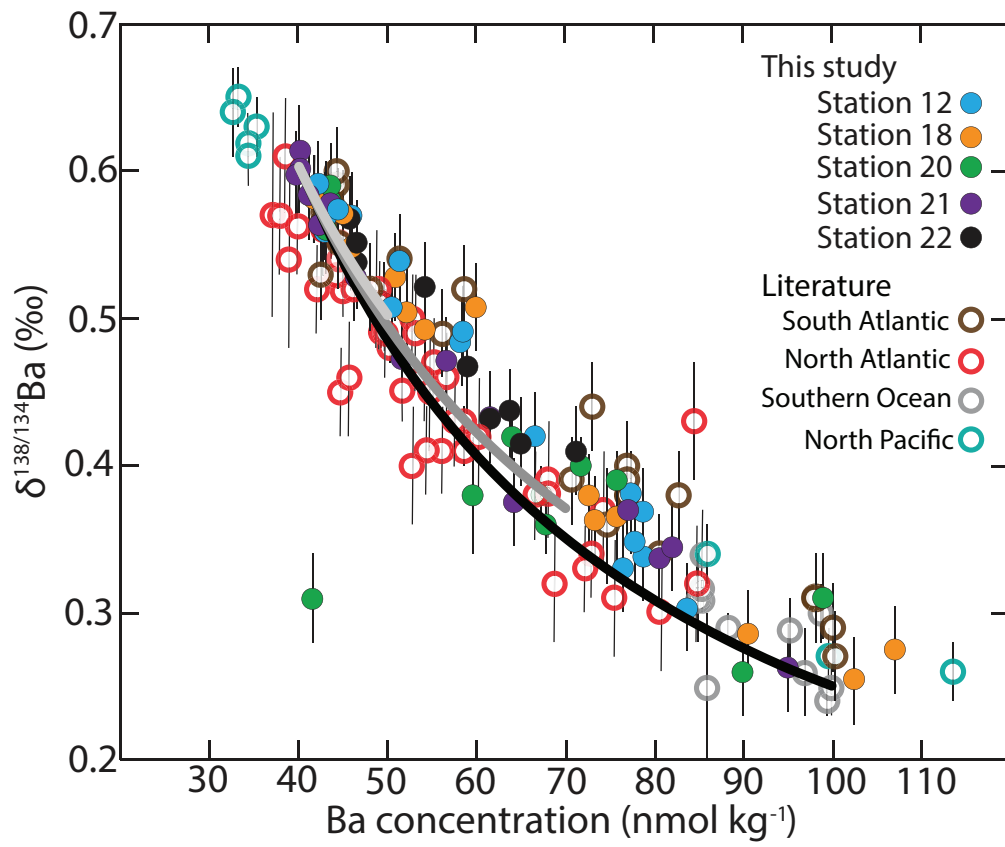


Figure 7

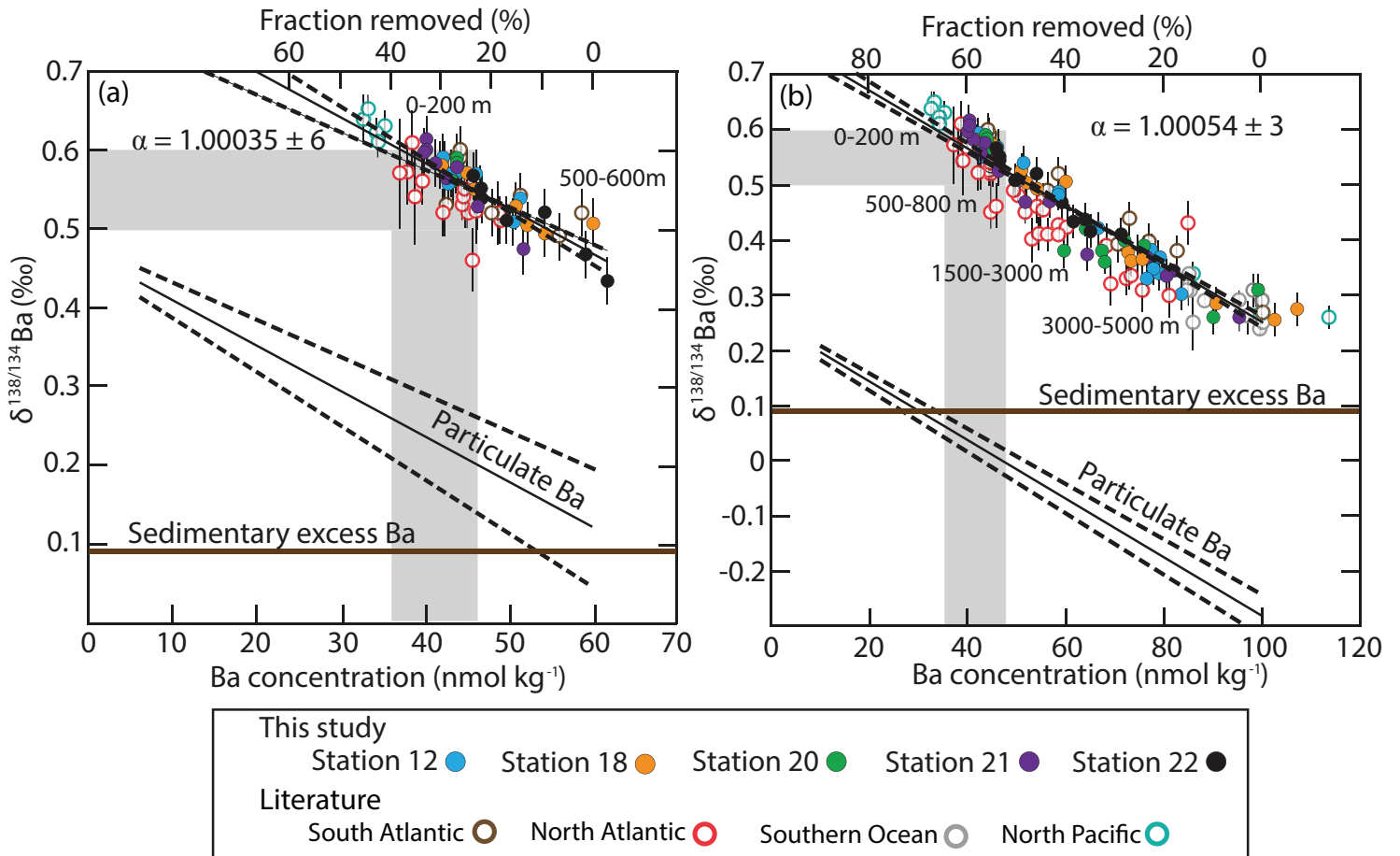


Figure 8

